Development of 12.5/25 GHz Optical Interleaving Filter Module with Isolator Function

研究論文

Development of 12.5/25 GHz Optical Interleaving Filter Module with Isolator Function

Hiroshi MATSUURA*

Abstract: Recently, wavelength-division multiplexing (WDM) technology has been adopted for configuring large-capacity metro/core fiber-optic communications networks. Accordingly, bandwidths are becoming narrower to obtain higher densities on communication wavelengths. Consequently, optical interleaving filters are necessary to demultiplex a single input to separate alternate wavelengths into individual outputs. By developing a proprietary configuration, the authors have succeeded in developing an optical interleaving filter that does not require temperature control.

Keywords: Interleaving filter, Optical isolator, Wavelength-division multiplexing, Polarization

1 Introduction

Since the mid 90s, the global demand for the construction of an information and telecommunication infrastructure increased. Since then optical telecommunication technology has progressed drastically [1]-[17]. Optical fiber networks without optical dispersion were constructed over 35 years ago, and they remain available and are sufficient for transmitting signals at speeds of up to 2.5 Gbps. Many carriers are installing additional 10 Gbps optical transmission devices into unused dark fiber and dark channels to raise the transmission capacity. If the wavelength interval of the signal light can be divided more finely, a practical system, such as the 256 ch×5 Gbps system depicted in Fig. 1 , is equivalent to an ultrahigh-speed communication system, such as a 32 ch×40 Gbps.

The proposed system is expected to reduce the initial cost, because the chromatic dispersion (CD) and the polarization mode dispersion (PMD) is less subjected for low communication speed, and existing optic-fiber cables and cheap transmission devices can be used. Various studies have examined this problem [18]-[22]. Therefore, we developed an integral component, called the interleaver, for the ultra dense wavelength-division multiplexing (DWDM) system, which divides the multiplex signal into groups of even and odd numbers of wavelengths at 25 GHz intervals. Moreover, two groups of even and odd numbers of wavelengths can be combined to multiplex signals at 12.5 GHz intervals. The present study describes the configuration of the component and reports the properties of fabricated prototypes.

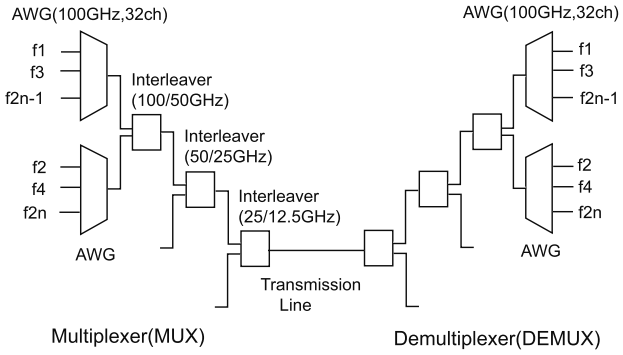

Fig. 1: The system chart for ultra DWDM.

* Tohoku Gakuin University, Faculty of Engineering, Department of Mechanical Engineering and Intelligent Systems

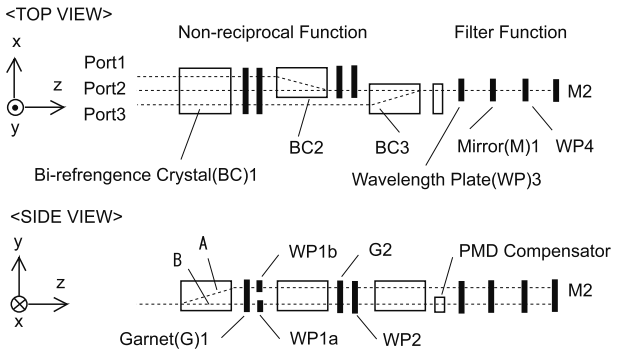

Fig. 2: Sutructure of new interleaver.

2 System Principle

The developed interleaver (Fig. 2) comprises input/output fibers, a hermetic package, a newly fabricated non-reciprocal function, a flat top transmission band, and a filter function using several optical crystals and an etalon to achieve miniaturization [23]. Moreover, the interleaver offsets the PMD using a PMD compensator because the developed interleaver has PMD caused by the optical path difference between rays A and B in BC1 (birefringence crystal).

2.1 Non-reciprocal Circuit

The non-reciprocal device has several abilities and processes, which are discussed below. First, the non-reciprocal device converts two mutually perpendicular polarizations into two mutually parallel polarizations. Secondly, two parallel polarization lights enter the Gires-Tournois interferometer (GTI) function without changing the deviation angle of the progress direction and returns to the non-reciprocal function precisely after having repeated the internal filter function. Thirdly, the non-reciprocal device can easily perform multiplexing and de-multiplexing by reversing the optical axial angle of the $\lambda/2$ wavelength plate. Additionally, the behavior of the non-reciprocal device is unchanged, even if the order of the $\lambda/2$ wavelength plate adjacent to the garnet crystal is exchanged. The conversion process of polarized light for the demultiplexer is in Fig. 3.

The light that entering Port 2 is converted into two polarized lights that are made parallel to the

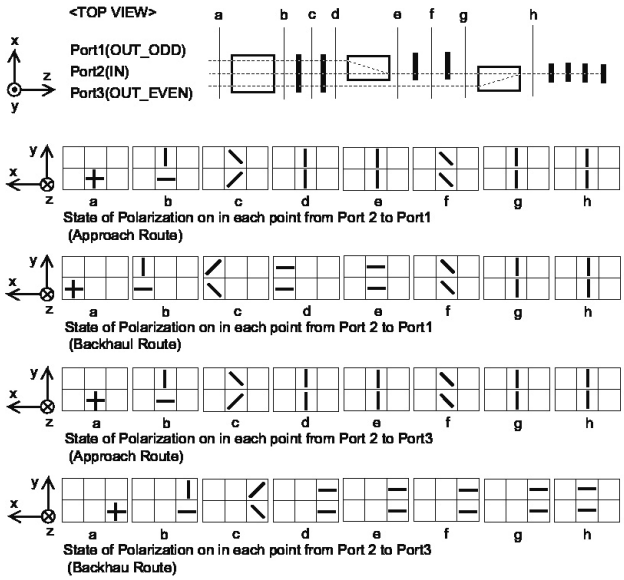

Fig. 3: Statements of polarization and optical propagations of non-reciprocal function of the interleaver (De-multiplexer type).

y-axis after passing through the non-reciprocal device. Subsequently, the lights enter the GTI function. The refracted lights from the GTI function are divided into polarized lights having an odd number of wavelengths that are parallel to the y-axis. Meanwhile, the polarized lights having an even number of wavelengths are parallel to the x-axis. Two polarized lights for each group of odd numbered wavelengths pass a BC3 (Birefrengence Crystal) as an ordinary ray and rotate 90° by a WP2 (wavelength plate) and a G2 (garnet). These lights pass a BC2 as an extraordinary ray, and the optical propagation is shifted to the side of Port 1.

Mutually parallel polarized lights are changed to perpendicular polarization using a WP1 and a G1. The perpendicular polarized lights are mixed by a BC1 and passed to Port 1. A group of lights with an even-numbered wavelength passes a BC3 as an extraordinary ray. Accordingly, propagation of light shifts to the Port 3 side. Following the conversion into perpendicular polarized light by a WP1 and a G1, two beams are combined into a single beam by a BC1 and passed to Port 3 [24].

2.2 GTI with retardation film

It is impossible to achieve the characteristics of the flat top transmission band using the solid etalon for the interleaving device and increasing the finesse to reduce the cross talk of the adjacent wavelength. Therefore, we have realized the flat top using a non-reciprocal function and a GTI filter function. The transmission spectrum can be obtained from the electric field intensity E_{in} to be incident on the GTI using the Jones matrix shown below:

$$
\begin{aligned}
&E_{\mathrm{out}} = M_{\mathrm{wp}} \cdot M_{\mathrm{GTI}} \cdot M_{\mathrm{wp}} \cdot E_{\mathrm{in}} = \\
&\begin{pmatrix} \cos\alpha & -\sin\alpha \\ \sin\alpha & \cos\alpha \end{pmatrix}
\begin{pmatrix} A & 0 \\ 0 & B \end{pmatrix}
\begin{pmatrix} \cos\alpha & -\sin\alpha \\ \sin\alpha & \cos\alpha \end{pmatrix} \\
&\begin{pmatrix} \cos\beta & -\sin\beta \\ \sin\beta & \cos\beta \end{pmatrix}
\begin{pmatrix} \frac{r_1+r_2C}{1+r_1r_2C} & 0 \\ 0 & \frac{r_1+r_2D}{1+r_1r_2D} \end{pmatrix} \\
&\begin{pmatrix} \cos\beta & -\sin\beta \\ \sin\beta & \cos\beta \end{pmatrix} \\
&\begin{pmatrix} \cos\alpha & -\sin\alpha \\ \sin\alpha & \cos\alpha \end{pmatrix}
\begin{pmatrix} A & 0 \\ 0 & B \end{pmatrix}
\begin{pmatrix} \cos\alpha & -\sin\alpha \\ \sin\alpha & \cos\alpha \end{pmatrix} \\
&\begin{pmatrix} E_x \\ E_y e^{j\phi} \end{pmatrix}. \qquad (1)
\end{aligned}
$$

$$
\begin{aligned}
A &= e^{-j\frac{2\pi}{\lambda}(t_{\mathrm{wp}}n_{\mathrm{o}})}, \\
B &= e^{-j\frac{2\pi}{\lambda}(t_{\mathrm{wp}}n_{\mathrm{e}})}, \\
C &= e^{-j\frac{4\pi}{\lambda}(t_{\mathrm{air}}n_{\mathrm{air}}+t_{\mathrm{wp}}n_{\mathrm{o}})}, \\
D &= e^{-j\frac{4\pi}{\lambda}(t_{\mathrm{air}}n_{\mathrm{air}}+t_{\mathrm{wp}}n_{\mathrm{e}})}.
\end{aligned}
$$

$$
\begin{aligned}
&(n_{\mathrm{air}}-1)\times 10^8 = \Big\{2371.34 + \frac{683939.7}{130-\nu^2} + \\
&\frac{4574.3}{38.9-\nu^2}\Big\}D_{\mathrm{s}} + (6487.31 + 58.058)\nu^2 \\
&-0.7115\nu^4 + 0.08851\nu^6)D_{\mathrm{w}}, \qquad (2) \\
&D_{\mathrm{s}} = \frac{P_{\mathrm{s}}}{T_{\mathrm{temp}}}\Big\{1 + P_{\mathrm{s}}\Big(57.9\times 10^{-8} \\
&-\frac{9.325\times 10^{-4}}{T_{\mathrm{temp}}} + \frac{0.25844}{T_{\mathrm{temp}}^2}\Big)\Big\}, \\
&D_{\mathrm{w}} = \frac{P_{\mathrm{w}}}{T_{\mathrm{temp}}}\Big\{1 + P_{\mathrm{w}}\Big[1 + 3.7\times 10^{-4}P_{\mathrm{w}}\Big]\times \\
&\Big[-2.37321\times 10^{-3} + \frac{2.23366}{T_{\mathrm{temp}}} + \frac{710.792}{T_{\mathrm{temp}}^2} \\
&+\frac{7.75141\times 10^4}{T_{\mathrm{temp}}^3}\Big], \\
&\nu = 1/\lambda.
\end{aligned}
$$

where electric fields in the x-axis and y-axis directions are denoted as E_x and $E_y e^{j\phi}$ denote the electric fields in the x-axis and y-axis, respectively, respectively, ϕ denote the retardation between E_x and E_y, α represents the angle between the optical axis of WP3 and the x-axis, β denotes the angle between the optical axis of WP4 and the x-axis.

Additionally, the rotation matrix is used to match the coordinate of an electric field with the axis direction of a quarter-wavelength plate. After calculating the retardation in the GTI, the coordinate is returned to the original coordinate using an inverse rotation matrix. Here, r_1 and r_2 denote the reflection ratios of the etalons, t_{air} denotes the thickness of air, n_{air} corresponds to the index of air, t_{wp} represents thickness of the wavelength plate, and n_o and n_e denote the indices of the ordinary and extraordinary wavelength plates [25],[26].

Using Eq. 1 and Owens's Eq. 2, the transmission spectrum and the temperature characteristic are illustrated in Fig. 4 [27]. Here, P_{s}(hPa) denotes the pressure of standard air and P_{w}(hPa) indicates the pressure of vapor. The transmission spectrum of an odd number wavelength expressed by a solid line and two dotted lines at an operating temperature range of 0 - 70°C. For reference, the transmission spectrum of an even number wavelength is indicated by a chain line. We have stabilized the fluctuation of the wavelength of a distributed feedback (DFB) laser source to be less than 10 pm, which is indicated by the bold frame line, using an external wavelength locker. Besides, the cross-talk of an adjacent wavelength should exceed 20 dB to perform high-quality communications.

Even if glass-ceramic with an extremely low thermal expansion coefficient, such as ZERODUR (by Schott Glass), is used for the GTI, a transmission spectrum shift by temperature exists from its thermal expansion coefficient. Hence, it is necessary to control the temperature of the GTI by the Peltier effect or adopt a structure to cancel out the temperature shift.

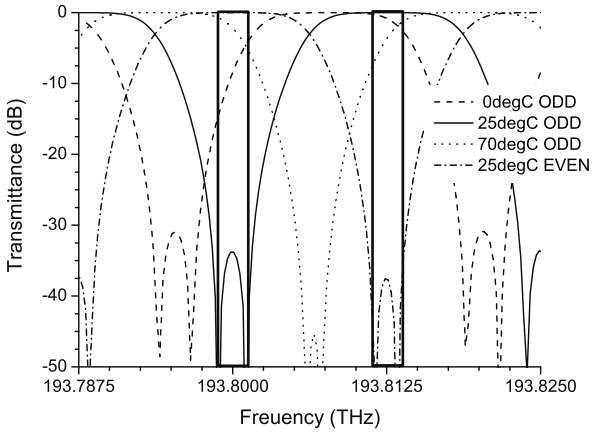

Fig. 4: Calculated characteristics of temperature changing of the interlever at 25°C and 1013 hPa.

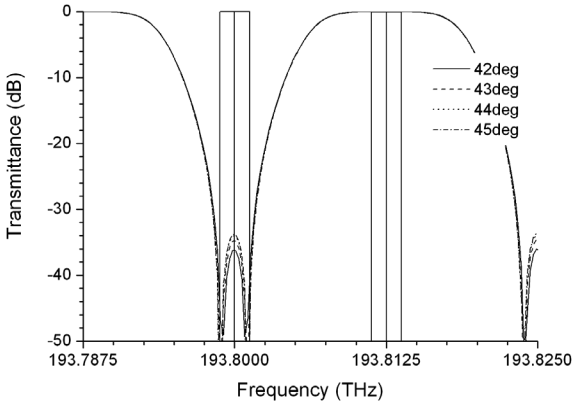

Fig. 5: Calculated transmission spectrum change by erorr of an optical axis of the $\lambda/8$ wavelength plate at 25°C and 1013 hPa.

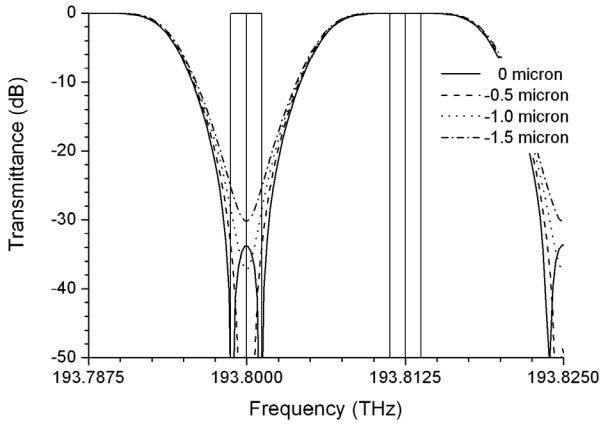

Fig. 6: Calculated transmission spectrum change by the errorr of a thickness of the $\lambda/8$ wavelength plate at 25°C and 1013 hPa.

2.2.1 Transmission spectrum change by the condition of the $\lambda/8$ wavelength plate

Lights pass through a zeroth-order $\lambda/8$ wavelength plate made of the synthetic quartz before entering the GTI. The thickness error and the angle of the wavelength plate occur during production: For example, during the dicing of the wavelength plate or assembly. The accuracy of the mounting angle and thickness are less than 2.5 degrees and approximately 0.5 microns. The calculated results for the error in the angle and the thickness are presented in Figs. 5 and 6, respectively. The influence of an optical axis error was calculated by changing the optical axis angle of the wavelength plate from 42 degrees to 45 degrees.

It is possible to process and assemble to an accuracy of 2.5 degrees. Thus, the transmission spectrum is unaffected by the angle error of the $\lambda/8$ wavelength plate provided by the conventional method. A difference in thickness may be assumed to affect retardation and disturb transmission spectrum.

2.2.2 Transmission spectrum change by the condition of the $\lambda/4$ wavelength plate

Similarly, the change in the transmission spectrum by the error of the optical axis in the $\lambda/4$ wavelength plate is shown in Fig. 7.

The optical axis is varied from 43 - 45 degrees corresponding to the error provided by the conventional processing method. Fig. 8 shows the change in the transmission spectrum by the thickness error of the $\lambda/4$ wavelength plate. The calculation result indicated that the transmission spectrum shift is caused by the thickness error of the $\lambda/4$ wavelength plate throughout the C-Band. Therefore, this device must compensate for temperature.

2.2.3 Influence of atmospheric pressure

Quartz and air are the only materials in the optical path of the GTI. As described above, the transmission spectrum is shifted by the difference in the optical path in the GTI. It is because of the temperature dependence of quartz and the

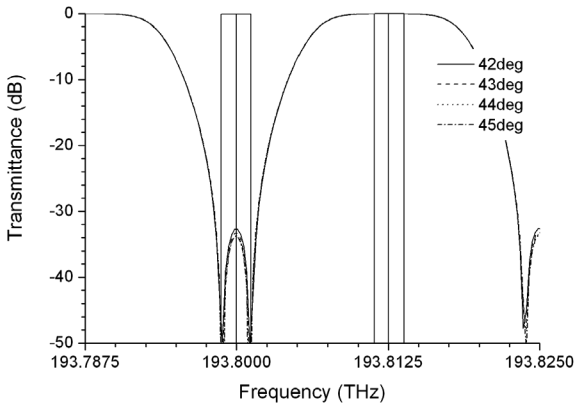

Fig. 7: Calculated transmission spectrum change caused by the error of an optical axis of the $\lambda/4$ wavelength plate at 25°C and 1013 hPa.

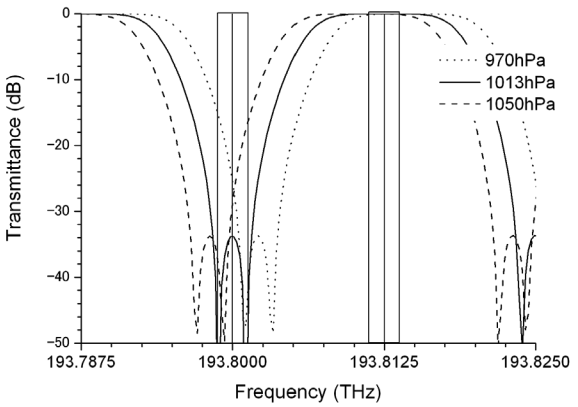

Fig. 9: Calculated transmission spectrum change due to atmospheric pressure (1013.25 hPa) at 25°C.

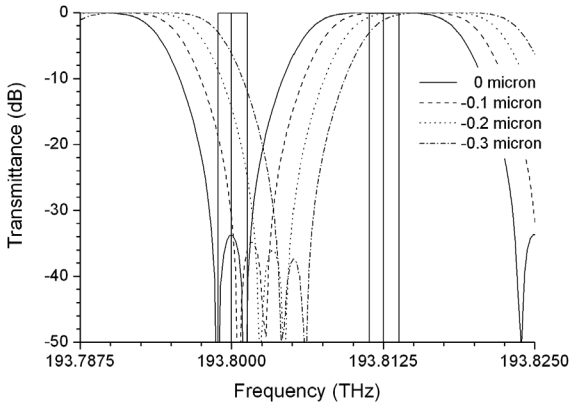

Fig. 8: Calculated transmission spectrum change caused by the erorr of a thickness of the $\lambda/4$ wavelength plate at 25°C and 1013 hpa.

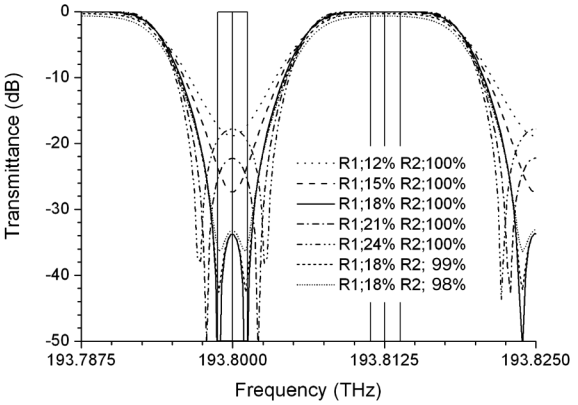

Fig. 10: Transmission spectrum change by a difference of reflectance of R1 mirror.

change of the refraction index of air caused by the atmospheric pressure change, as in Fig. 9 [25, 26]. The transmission spectrum is shifted by the change in atmospheric pressure owing to differences in weather and/or altitude. Therefore, the GTI part of all interleavers must be hermetically sealed.

2.2.4 Transmission spectrum change by mirror reflectance

Mirrors M1 and M2 have a reflectance of R1 and R2 respectively, and the GTI is made of a dielectric thin film form composed of SiO_2 and Ta_2O_5. Since both mirrors are designed to have an incidence angle of 0 degrees, there is no polarization dependence. Therefore, it is easy to design arbitrary reflectance and generate a flat reflectance in the operating wavelength range. The reflectance of R1 is a critical parameter that determines the transmission spectrum and suppression ratio. Figure 10 illustrates that, a reflectance of 17 % to 19 % is sufficient. However, the film composition becomes complicated, and control of the film thickness becomes difficult resulting in an error of approximately 2 %. If the reflectance of R2 falls, the transmittance will drop remarkably. If the reflectance of R1 becomes smaller than 18 % then the transmission spectrum of the flat top will collapse.

2.2.5 Airtight structure of the interleaver

As mentioned before, the GTI must be hermetically sealed since changes in atmospheric pressure shifts the transmission spectrum. However,

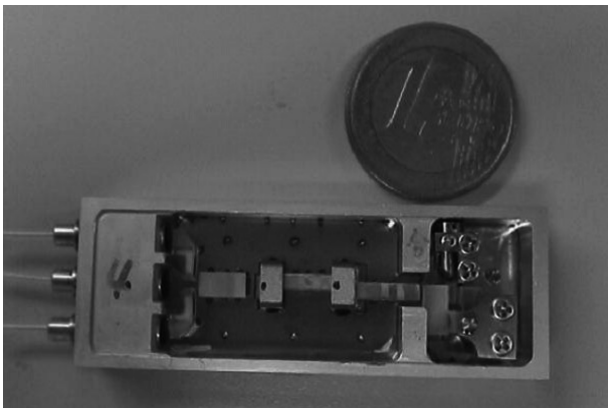

Fig. 11: Internal structure of Interleaver (Dimension is 20(W)×58(L)×9(T) mm).

the proposed interleaver has three collimators as input/output ports obtained by unification of the aspheric lens and the optical fiber. Since collimators have narrow intervals, stripping off the clothing material of the optical fiber of the collimator and applying the metal coating for soldering is difficult and is not cost effective. Therefore, only the non-reciprocal and GTI sections were hermetically sealed. An external view is presented in Fig. 11.

The case comprises two materials made by the simultaneous lost-wax process method. SUS304, which has good laser weld-ability, was used for the portion of the fiber input/output to perform laser welding between the collimator and the case. Fe-Ni-Co alloy, which has good seam weld-ability, was used for the area protecting the GTI section, which is seam welded between the lid and the case. Once the gilding processes were performed on the case manufactured via the lost-wax process, three sapphire windows were used to seal the hole of the input/output part of the light inside the case. This package has a structure in which a Peltier device is attachable to the bottom for temperature control of the GTI and the pins of the thermistor for measuring the temperature of the GTI can be inserted in the base of the package.

2.3 Compensation method of the GTI function

In the preceding subsection, it was mentioned that the transmission spectrum can be shifted using the linear expansion coefficient and refractive index temperature dependency of a $\lambda/4$ wavelength plate. For temperature compensation, fixed temperature control using the Peltier effect is a simple, straightforward approach. However, compensation without consuming electric power is ideal. Accordingly, we designed two methods, one uses the temperature characteristics of the crystal and the other uses the difference linear coefficient expansion and Young's modulus.

2.3.1 Temperature compensation method with optical glass

The requirement for the compensation is to cancel out the optical path length difference of quartz dn/dT within the GTI and the linear expansion coefficient of ZERODUR, which fixes the cavity mirror for the GTI. The optical path length in the GTI denoted by $nd(T)$ can be expressed as follows:

$$\begin{aligned} nd(T) = &\left(n_{\mathrm{air}}(T_0) + \frac{dn_{\mathrm{air}}}{dT}\Delta T\right)(t_{\mathrm{z}}(1 + a_{\mathrm{z}}\Delta T)) \\ &-t_{\mathrm{q}}(1 + a_{\mathrm{q}}\Delta T - t_{\mathrm{g}}(1 + a_{\mathrm{g}}\Delta T)) \\ &+t_{\mathrm{q}}(1 + a_{\mathrm{q}}\Delta T)\left(n_{\mathrm{e,o}} + \frac{dn_{\mathrm{e,o}}}{dT}\Delta T\right) \\ &+t_{\mathrm{g}}(1 + a_{\mathrm{g}}\Delta T)\left(n_{\mathrm{g}} + \frac{dn_{\mathrm{g}}}{dT}\Delta T\right). \end{aligned}$$

where $\frac{dn_{\mathrm{air}}}{dT}$ denotes the temperature-dependent coefficient of the air refractive index, t_{z} denotes the thickness of ZERODUR, a_{z} represents the linear expansion coefficient of ZERODUR, t_{q} corresponds to the thickness of the wavelength plate, a_{q} denotes the linear expansion coefficient of the wavelength plate, $n_{\mathrm{e,o}}$ indicates the refraction index of the wavelength plate, $\frac{dn_{\mathrm{e,o}}}{dT}$ denotes the temperature dependence coefficient of the wavelength plate, t_{g} corresponds to the thickness of the compensator plate, a_{g} indicates the linear expansion coefficient of the compensator plate, n_{g} corresponds to the refraction index of the compensator plate, $\frac{dn_{\mathrm{g}}}{dT}$ symbolizes the temperature dependence coefficient of the compensator plate.

$$\lim_{T \to T_0} \frac{nd(T) - nd(T_0)}{T - T_0} = 0. \tag{3}$$

If Eq.(3) is solved with respect to t_{g} by omitting the temperature characteristic of air and a

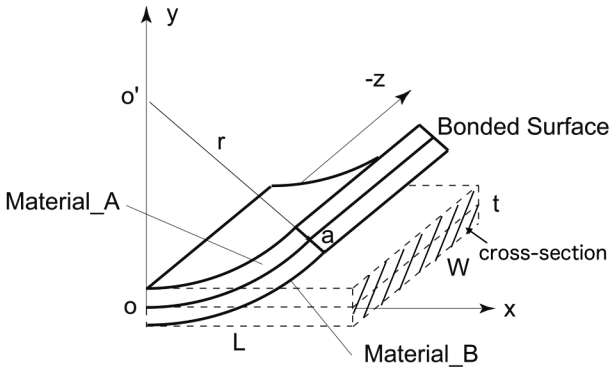

Fig. 12: Structure of temperature compensation using bi-metal.

high-order term, the following equation is obtained:

$$t_{\mathrm{g}} = \frac{n_{\mathrm{air}}(T_0) \cdot t_{\mathrm{z}} \cdot a_{\mathrm{z}} + t_{\mathrm{q}} \cdot E}{n_{\mathrm{air}}(T_0) \cdot a_{\mathrm{g}} - \frac{dn_{\mathrm{g}}}{dT} - a_{\mathrm{g}} \cdot n_{\mathrm{g}}}, \quad (4)$$

$$E = \frac{dn_{\mathrm{e,o}}}{dT} + a_q(n_{\mathrm{e,o}} - n_{\mathrm{air}}(T_0)).$$

BK7 is the material for the compensator. This temperature compensation method has an advantage in reliability owing to a lack of moving parts. However, there is also a drawback in that the precise angle adjustment of BK7 must be performed during the initial stage.

2.3.2 Mechanical compensation method with the bimetallic method

Fig. 12 shows temperature compensation by a bimetallic plate comprising materials having different linear expansion coefficients and Young's module.

When the temperatures of two materials change identically, one material expands compared with the other materials. Since the movement of the curvature is fixed and is restricted by the respective materials, the material for which the side open to the air is concave and has the smaller coefficient of expansion. There is no force due to the bimetallic plate, and the internal force on the bimetallic plate of the two materials is balanced.

The cross-section shape is independent of temperature changes. If the bimetallic plate is curved evenly around o′, θ and e are given as follows:

$$\theta = \frac{(1+e_0)L}{r} = \frac{(1+e)L}{r-y}. \quad (5)$$

The fractional forms of the backward term in this equation are rearranged, as shown by the following relationship between strain and bending:

$$e = e_0 - \frac{(1+e)L}{r}y. \quad (6)$$

The equation relating to temperature change is expressed using the superposition principle, and α_n,Δ T, s and E_n are given as follows:

$$e = \alpha_n \Delta T + \frac{s}{E_n}. \quad (7)$$

Where r denotes the bending radius, e_0 denotes the strain at an aspect joining two materials, e represents the strain at this point, L denotes the length of the material in the y direction, w corresponds to the length of the material in the z direction, t corresponds to the thickness of the material, α_n is the coefficient of linear expansion, ΔT denotes the difference in temperature, θ is the angle of o-o'-a, s symbolizes the stress, and E_n corresponds to Young's modulus.

The stress should be a function of the position in the cross section. Therefore, Eq. 7 is solved for stress and Eq. 6 is substituted for e to obtain the following equation:

$$s = E_n(e_0 - \alpha_n T) - E_n\left(\frac{1+e_0}{r}\right)y. \quad (8)$$

Therefore, there is no composite force acting perpendicular to the cross-section. It means that the integral of the stress on the cross section is zero, as indicated by the following:

$$\int_{-t/2}^{t/2} sw\, dy = 0. \quad (9)$$

Furthermore, there is no external force, and since there is no moment across the cross-section, Eqs. 9 and 10 are satisfied.

$$\int_{-t/2}^{t/2} swy\, dy = 0. \quad (10)$$

When Eqs. 5 and 6 are considered as the fundamental parameters, and integrated and expanded, the following equations are obtained:

$$e_0 = \frac{\frac{\alpha_1 E_1}{E_2} + \frac{\alpha_2 E_2}{E_1} + 7(\alpha_1 + \alpha_2)}{\frac{E_1}{E_2} + \frac{E_2}{E_1} + 14} \Delta T, \qquad (11)$$

$$\frac{1 + e_0}{r} = \frac{24(\alpha_2 - \alpha_1)}{\left(\frac{E_1}{E_2} + \frac{E_2}{E_1} + 14\right) t} \Delta T. \qquad (12)$$

From the results of these equations, we designed a mechanism to compensate for the variation in temperature using Cu-Ni-Mn and Ni-Fe materials having1 mm length and a 0.1 mm thickness.

2.4 PMD and CD

If the PMD and CD are extensive, then the interleaver degrades the transmission quality. Regarding the PMD, the optical path difference of crystals caused primarily by the rutile (TiO_2) or the YVO_4 (Yttrium orthovanadate) in a non-reciprocal device can be compensated for by a compensator composed of BK7. Additionally, the wavelength plate in the GTI also has an optical path difference; however, the refractive index difference related to the thickness of the quartz can be neglected. As for the CD, the non-reciprocal device does not have retardations. However, the GTI has some CD. Therefore, the calculated group delay and dispersion from the following equations are in Figs. 13 and 14:

$$\phi = argE. \qquad (13)$$

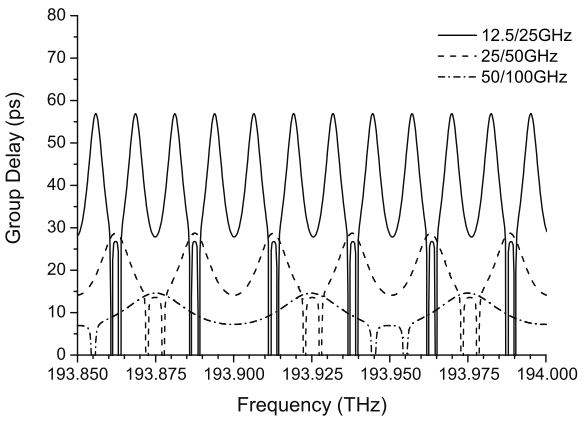

Fig. 13: Calculated group delay of the interleaver.

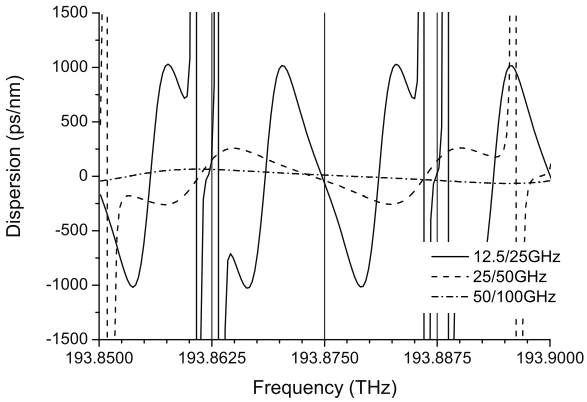

Fig. 14: Calculated CD of the interleaver.

$$\tau = \frac{d\phi}{d\omega} = \frac{\lambda^2}{2\pi c} \frac{d\phi}{d\lambda}, \qquad (14)$$

$$D_s = \frac{d\tau}{d\lambda}. \qquad (15)$$

where ϕ denotes the phase response, ω corresponds to the frequency, τ denotes the group delay, c corresponds to the speed of light, λ denotes the wavelength, and D_s denotes the dispersion.

The period of the wavelength has a profound effect on the dispersion and the group delay. However, its influence is relatively small, when the transmission speed is slow.

3 Experimentation and Considerations

In the case of the multiplexer, when a group of odd-numbered wavelengths and a group of even number wavelengths are incident in Port 1 and Port 3, respectively, the combined light emerges from Port 2. The propagation of the demultiplexer is in the opposite direction to the multiplexer. The characteristics for each measurement condition are described in the following sections.

3.1 Characteristics of the interleaver

The transmission spectrum, the cross talk, the isolation, and the temperature dependent loss (TDL) of the interleaver as a stand-alone were measured using a tunable light source, an optical spectrum analyzer, and an optical power meter. Matching oil is applied to one end of a fiber that is not use for the measurement to prevent the influence of returning light.

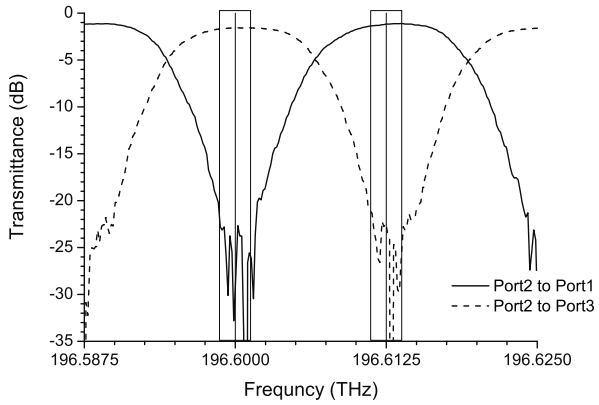

Fig. 15: Transmission spectrum of the demultiplexer at shorter wavelength.

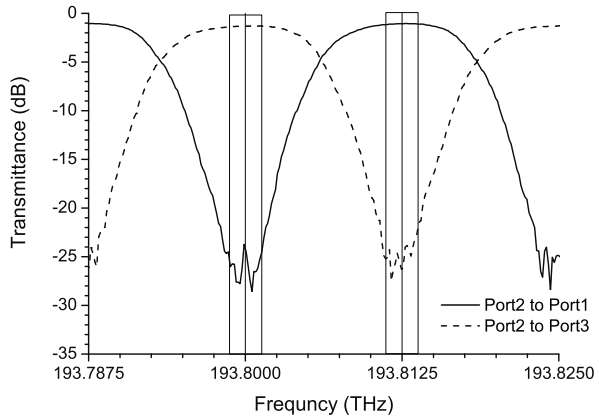

Fig. 16: Transmission spectrum of the demultiplexer at middle wavelength.

3.1.1 Transmission spectrum

The transmission spectrums of the shorter wavelength to the longer wavelength of the demultiplexer are in Figs. 15, 16, and 17. In the wavelength range of 1525 - 1565 nm, the transmission spectra of Port 1 and Port 3 each exhibit periodic cycles of 12.5 GHz with the characteristics of a center wavelength. Besides, the characteristics of the insertion loss, which is defined for the loss between the input and output fibers of the module, is less than 1.5 dB, as obtained by both the multiplexer and the demultiplexer. Besides, the polarization dependent loss (PDL) within 5 pm of the center wavelength was less than 0.2 dB. However, the signal-to-noise ratio was low for the expected performance. It is attributable to a number of accumulations, such as

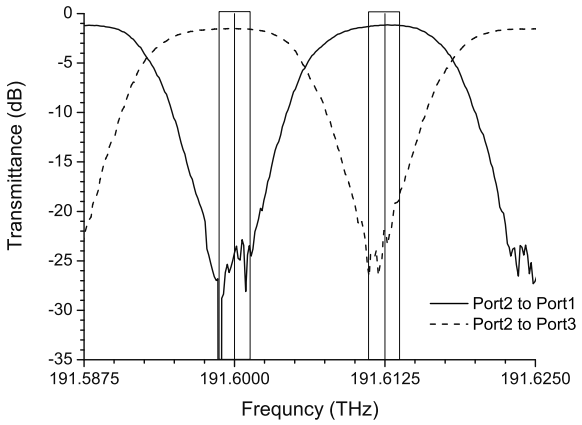

Fig. 17: Transmission spectrum of the demultiplexer at longger wavelength.

Table 1: Difference in compensation of resonance length with and without sealed structure

Hermetic / Type	Before	After
BK7	1	0.36
Bi-metal	1.3	0.1

[Units: pm/°C]

the scattering at all vacuum-deposited thin film interfaces and the phase leg of the crystals. To solve this problem, it is better to connect the interleaver and the comb filter in series, which removes the unwanted ports from the interleaver.

Furthermore, the result of the measured stability of the center wavelength by two temperature compensation methods is listed in Table 1. The value was obtained by measuring the shifted full width at half maximum (FWHM) while changing the temperature of the module. The shift of the FWHM was measured using the optical spectrum analyzer while changing the temperature.

3.1.2 Isolation

The isolation function is a main advantage of this interleaver, which is unavailable in other types of interleaver. The characteristics of the isolation in each port are illustrated in Fig. 18. High isolation, over 45 dB, was obtained at a range of operation wavelengths of from 1525 - 1565 nm. The retardation error of the wavelength plate and the angle error of the optical

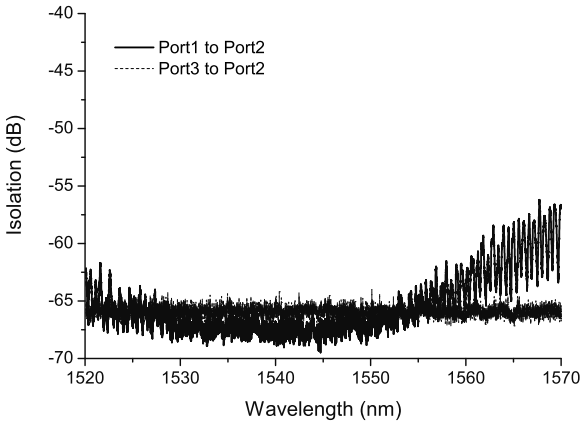

Fig. 18: Characteristic of the isolation.

Table 2: Results of Return Loss

	Port 1	Port 2	Port 3
Mux-type	-54.7	-55.2	-54.2
Demux-type	-55.6	-53.5	-56.1

[Units: dB]

axis of the wavelength plate are the main reasons for the poor isolation on the longer wavelength side.

3.1.3 Return Loss

The histogram of the return loss in each port is presented in Table 2. The characteristics of the return loss are excellent for all ports.

3.2 Reliability Test

We performed a series of reliability tests, which refer to the Telcordia1209, such as the heat cycle test, the vibration test, and the impact test. Since this interleaver is hermetically sealed to protect the optical parts and avoid condensation and exposure to water, we did not perform the damp heat test. The examination condition and its results are listed in Table 3. In all the examinations, the characteristics of the interleaver did not deteriorate, and the interleaver was proved to have sufficient reliability.

Table 3: Results of Reliability Test

Item / Test	Loss Variation	Critetia
Heat Cycle	-0.1	$<$ -0.5
Impact	-0.12	$<$ -0.5
Vibration	-0.05	$<$ -0.5

[Units: dB]

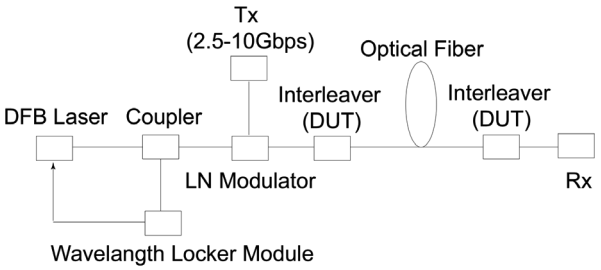

Fig. 19: Setup for the transmission experiment.

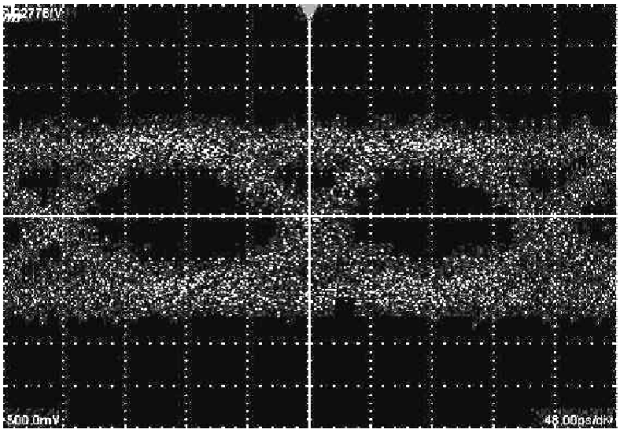

Fig. 20: Eye pattern of 5 Gbps transmission.

3.3 Transmission test of the 12.5/25 GHz interleaver

We performed a 5 Gbit/s transmission experiment with the interleaver (DUT: Device Under Test). The experimental system is illustrated in Fig. 19. The performance of the 25 GHz wavelength locker module integrated DFB laser developed herein was upgraded to 12.5 GHz. Moreover, the accuracy of the wavelength locker was 1.5 pm from -5 - 60°C. The stability of the transmission spectrum of the interleaver, which is a filter with an extremely narrow band, must be lower than 5 pm. The lithium niobate modulator was modulated using 5 Gbps and 10 Gbps digital signals. The eye pattern of 5 Gbps transmission is depicted in Fig. 20. Here, there was no loss of sharpness in an eye pattern until 5 Gbps, and transmission was impossible for 10 Gbps.

4 Conclusion

A practical 12.5/25 GHz interleaver having a small insertion loss and dimensions with a TDL of a transmission profile of less than 1 pm/°C has been developed. This component was experimentally proven to be capable of transmitting at speeds of up to 5 Gbps. Based on the results of the present study, systems may be capable of operating at 1.28 Tbps or 5 Gbps × 256 channels using the proposed interleaver.

Acknowledgement

I would like to thank M. Yamagaki S. Wako and S. Abe for technical assistance with the experiments. I would also like to thank D. Yoon for lending his expertise on the application of optical dispersion management and optical transmission techniques.

References

[1] G. Gharlet et al.: 3.2Tbit/s (80x42.7 Gb/s) C-band transmission over 9x100km of TeraLight fiber with 50GHz channel spacing, OAA'02, **PDP1** (2002).

[2] H. Sugahara et al.: 9,000-km transmission of 32 x 42.7 Gb/s dense-WDM signals using 195-$\mu m^2 A_{eff}$ fiber and inverse double-hybrid span configuration, OAA'02, **PDP3** (2002).

[3] N. Sugimoto et al.: Highly efficient and short length Lanthanum co-doped Bi_2O_3 based EDF for extended L-band amplification, OAA'02, **PDP5** (2002).

[4] B. Zhu et al.: Transmission of 3.2 Tb/s (80 x 42.7 Gb/s) over 5,200km of UltraWave fiber with 100-km dispersion-managed spans using RZ-DPSK format, ECOC'02, **PD4.2** (2002).

[5] K. Shimizu et al.: Fiber-effective-area managed fiber lines with distributed Raman amplification in 1.28-Tb/s (32 x 40 Gb/s) 202-km unrepeated transmission, Technical Digest of OFC2001, **TuU2** (2001).

[6] T. Miyazawa et al.: A study of noise reduction in distributed fiber Raman amplification, Technical Digest of CLEO/Pacific Rim'01, **ThB1-2** (2001).

[7] H. Ishikawa et al.: Polarization mode dispersion characteristics of various high performance optical fiber in cable, Proceedings of IWCS2001, paper, 12-7, pp506-513.

[8] M. Shirai et al.: Impedance-controlled-electrode (ICE) semiconductor modulators for 1.3μm 40-Gbit/s tranceivers, ECOC'02, **9.5.4** (2002).

[9] T. Tanaka et al.: High-sensitivity 40-Gb/s receiver with a wideband InAlAs waveguide avalanche photodiode, ECOC'02, **10.5.1** (2002).

[10] C. Bornholdt et al.: Novel all-optical 3R regenerator concept demonstrated at 40 Gbit/s, ECOC'02, **PD4.8** (2002).

[11] M. Tur et al.: Modules for chromatic dispersion and dispersion slope management, OFC'02, **TuT4** (2002).

[12] T. Sugihara et al.: Automatically tracked dispersion compensation with penalty-free tunable dispersion equalizer for 40 Gbit/s systems, OFC'02, **TuAA2** (2002).

[13] S. Ramachandran et al.: Wavelength-continuous broadband adjustable dispersion compensator using higher order mode fibers and switchable fiber-gratings, ECOC'02, **PD2.6** (2002).

[14] C.K. Madsen et al.: Integrated waveguide allpass filter tunable dispersion compensator, OFC'02, **TuT1** (2002).

[15] D.J. Moss et al.: Multichannel tunable dispersion compensation using all-pass multicavity etalons, OFC'02, **TuT2** (2002).

[16] Y. Painchaud et al.: Multi-channel fiber bragg gratings for dispersion and slope compensation, OFC'02, **TuAA5** (2002).

[17] Z. Pan et al.: Tunable chromatic dispersion compensation in a 4 x 40-Gbit/s system using sampled nonlinearly-chirped fiber Bragg gratings (NC-FBGs) ECOC'02, **10.3.3** (2002).

[18] Benjamin B. Dingel and Masayuki Izutsu: Multifunction optical filter with a Michelson-Gires-Tournois interferometer for wavelength-division-multiplexed network system applications, Optics Letters, **23**, 14 (1998).

[19] S. Cao et al.: Birefringent Gires-Tournois interferometer (BGTI) for DWDM interleaving, OFC2002 **ThC3**, 1, (2002) 395.

[20] M. Oguma et al.: Passband-Width broadening design for WDM filter with Lattice-Form interleave filter and arrayed-waveguide gratings, IEEE Photonics Tech. Lett., **14**, 3, (2002).

[21] T. Kimura et al.: Temperature compensation of birefringent optical filter, Proceedings of the IEEE (1971).

[22] Benjamin B. Dingel and Tadashi Aruga: Properties of a novel noncascaded type, easy-to-design, ripple-free optical bandpass filter, Journal of Lightwave Technology, **17**, 8, (1999).

[23] Amnon Yariv and Pochi Yeh: *Optical Waves in Crystals* (Wiley New York).

[24] David S. Kliger, James W. Lewis and Cora Einterz Randall: *Polarized Light in Optics and Spectroscopy*(Academic Press,Inc).

[25] J.G.Old et al.: Dispersion of carbon dioxide J.Opt.Soc.Am., **61**, 89, (1971).

[26] M.J.Mace de Lepinay: J. phys., **1**, 23, (1892).

[27] J.C.Owens: Optical refractive index of air: dependence on pressure, temperature and composition Appl. Optics, **6**, 51, (1967).